Quantum Chemical Analysis of the Enolization of Ribulose Bisphosphate: The First Hurdle in the Fixation of CO_2 by Rubisco†

William A. King,‡ Jill E. Gready,*,‡ and T. John Andrews§

Computational Molecular Biology and Drug Design Group, John Curtin School of Medical Research, and Molecular Plant Physiology Group, Research School of Biological Sciences, Australian National University, Canberra ACT 0200, Australia

Received July 6, 1998; Revised Manuscript Received September 2, 1998

ABSTRACT: A study, using ab initio quantum chemical methods, of the first step in the reaction mechanism of Rubisco, the enolization of the substrate, ribulose bisphosphate, is reported. This is the first such study that takes into account the likely roles of critical features within the active site. On the basis of molecular dynamics relaxation of the complex between activated enzyme and substrate using X-ray crystallographic structures as starting coordinates, a 29-atom fragment that mimicked the active site was constructed. States along a proposed reaction pathway were calculated using density functional theory and Møller−Plesset second-order perturbation theory. The results are consistent with the postulate that the base that abstracts the C3 proton of ribulose bisphosphate is the metal-stabilized carbamate of Lys-201 formed during the activation process. The calculations suggest that the active-site residue, Lys-175, is charged before enolization commences and they indicate a possible means by which the enzyme directs the incoming CO_2 to attack the C2 carbon atom of the enediol, rather than the chemically very similar C3 atom.

D-Ribulose 1,5-bisphosphate (RuBP)[1] carboxylase/oxygenase (Rubisco) catalyzes the carboxylation or oxygenation of RuBP and the subsequent carbon−carbon cleavage to form two molecules of 3-phospho-D-glycerate (PGA) (with CO_2) or one molecule of PGA and one molecule of 2-phosphoglycolate (with O_2). The carboxylation reaction is the means by which CO_2 is acquired during photosynthesis, but the competing oxygenation reaction opposes it, resulting in the loss of both CO_2 and energy during the photorespiratory metabolism required to recycle the 2-phosphoglycolate (see refs *1*−*3* for reviews). Extensive experimental investigations have revealed many details of the reaction mechanism. The reaction involves several steps, each of complexity comparable with that of many other complete enzymatic reactions (*4*). The present study focuses on the initial step, the enolization of RuBP (Figure 1).

The conversion of the ketone form of RuBP to the enediol form requires removal of the proton from the carbon atom α to the carbonyl group and protonation of the carbonyl group. A specific active-site residue which acts as the proton-abstracting base (B in Figure 1) is a typical feature of enzymes that catalyze enolization, such as triosephosphate isomerase (*5*) and the enolase superfamily (*6*). It is not well established if an acidic group (A in Figure 1) is always required; electrostatic stabilization of the intermediate enolate may sometimes be sufficient. However, an acidic group is crucial to the Rubisco mechanism. The subsequent step in the reaction is the addition of CO_2 to the C2 atom. If the O2 atom was left unprotonated (i.e., in the enolate form), CO_2 addition would be incorrectly directed to the C3 atom. The identities of the acidic and basic groups involved in Rubisco-catalyzed enolization have not been established experimentally.

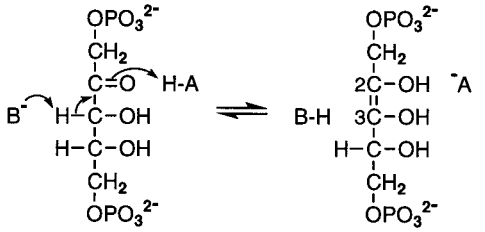

FIGURE 1: Enolization of RuBP. A proton must be removed from the C3 atom by a base (B), and an acid (A) must protonate the O2 atom.

Rubisco requires activation by carbamylation of the active-site residue Lys-201 before it is functional. Formation of this carbamate completes the coordination site for the magnesium ion, and the binding of magnesium stabilizes the carbamate. All known Rubiscos require carbamylation (see refs *1*−*3* for reviews). Crystallographic structures have been obtained with spinach and cyanobacterial Rubiscos in their activated forms and cocrystallized with an intermediate analogue, 2′-carboxyarabinitol bisphosphate (CABP)-(Rubisco.Mg^{2+}.Lys-201-CO_2.CABP; see Figure 2) (*7*, *8*). In

†This research was supported by an Australian National University (ANU) Strategic Development Grant, ANU Computing Equipment Committee Grant, and the ANU Supercomputer Facility.

* Author to whom correspondence should be addressed (e-mail Jill.Gready@anu.edu.au; fax +61 2 6249 0415).

‡ John Curtin School of Medical Research.

§ Research School of Biological Sciences.

[1] Abbreviations: RuBP, D-ribulose 1,5-bisphosphate; Rubisco, RuBP carboxylase/oxygenase; CABP, 2′-carboxyarabinitol 1,5-bisphosphate; 3KCABP, 3-ketocarboxyarabinitol bisphosphate; XuBP, xylulose 1,5-bisphosphate; PGA, 3-phospho-D-glycerate; DFT, density functional theory; MP2, Møller−Plesset second-order perturbation theory; RHF, spin-restricted Hartree−Fock; MD, molecular dynamics.

10.1021/bi981598e CCC: $15.00
Published on Web 10/14/1998

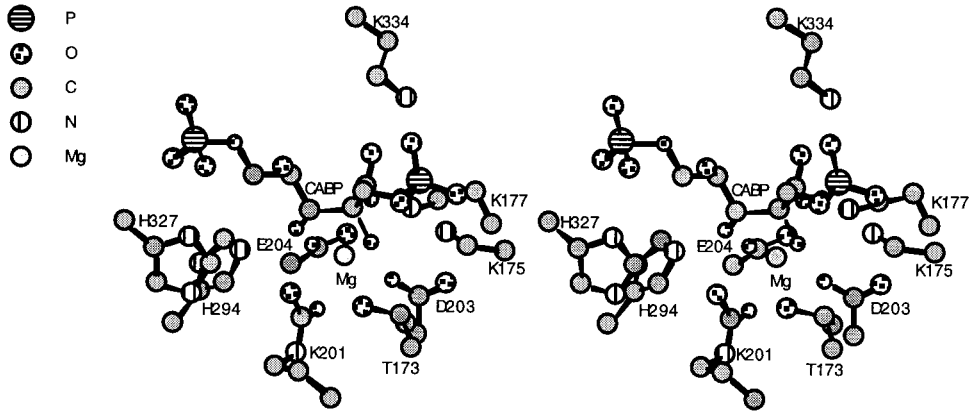

FIGURE 2: Stereoview of the active site of Rubisco. Coordinates were taken from the 1.6 Å X-ray crystal structure of ref *8*.

these structures, the only group suitably positioned to abstract the C3 proton is an oxygen atom of the carbamate formed during activation. Consequently, the carbamate has been proposed to be the proton abstracter (*4*, *7*, *8*). However, it is not clear that a carbamate group coordinated to a magnesium ion would be sufficiently basic to abstract a proton from the C3 atom of RuBP.

One aim of this study was to test whether this hypothesized role for the carbamate is feasible energetically. This is the first theoretical study of the reaction mechanism of Rubisco in which the effects of critical active-site residues have been modeled on the basis of X-ray structure coordinates. We have evaluated the proton-abstracting ability of the carbamate while it is coordinated to the magnesium ion. A suitable active-site fragment has been constructed that contains a portion of the substrate, RuBP, the metal, and several protein side chains that interact with these, including the lysyl carbamate. A proton-abstracting role is unprecedented for a protein carbamate. Therefore, our modeling included complementary studies with a metal-bound carbamate and with structurally similar metal-bound carboxylate groups. A carboxylate group of a glutamate residue fulfils the analogous proton-abstracting role in triosephosphate isomerase (*5*). The results suggest the Mg-coordinated carbamate group could be capable of functioning as the base in the enolization step and that this group is more basic than an analogously coordinated carboxylate.

Mutations at the Lys-175 position inactivate or seriously impair enolization but have less serious effects on other partial reactions (*9*). Therefore, Lys-175 must play an important role in the enolization of RuBP, and it was suspected initially that Lys-175 might be the base that abstracts the C3 proton (*9*, *10*). However, subsequent structural information precludes such an assignment (*11*, *12*). Lys-175 is quite remote from the position required for it to abstract the proton from the C3 atom. However, it is ideally positioned to protonate O2 of the enolate and also C2 of the subsequent *aci*-acid intermediate formed after C2−C3 bond cleavage (*13*). We have investigated the role played by Lys-175 in the enolization step by model calculations in which it is represented by both its cationic and neutral amino forms. The calculations suggest that this residue could play two important roles. Its protonated form appears first to stabilize the transition state for proton abstraction and second to act as the acidic group (A in Figure 1) that protonates O2 of the resultant enediolate.

METHODS

Programs. Calculations were run on a 20-node SGI Power Challenge XL and a 13-node Fujitsu VPP300 supercomputer. The AMBER 4.1 suite of programs (*14*) with the OPLS force field (*15*) was used for the molecular dynamics (MD) calculations. Gaussian 94 (*16*) was used for the quantum mechanical [spin-restricted Hartree−Fock (RHF) and Møller−Plesset second-order perturbation theory (MP2)] and density functional theory (DFT) calculations, with transition-state optimizations performed using the eigenvalue-following algorithm (*17*). A number of different basis sets were used to explore the requirements for representing negative charges (diffuse functions) and H bonding (polarization functions on hydrogen). Therefore, in addition to the 6-31G(d) basis set, 6-31+G(d) and 6-31+G(d,p) basis sets were used. Electron correlation contributions for states along the reaction pathway were evaluated by single-point calculations at MP2 level using RHF geometries optimized with the 6-31+G(d,p) basis set and by DFT calculations with geometry optimization using the three-parameter hybrid functional (B3LYP) of Becke (*18*) with the 6-31+G(d,p) basis set. The Hessian matrixes were calculated analytically at the optimized geometries of all states to verify that the correct number of imaginary frequencies were present.

Generation of the Initial Coordinates. Initial starting coordinates from the 1.6 Å X-ray crystal structure of activated Rubisco cocrystallized with CABP (Rubisco.Mg^{2+}.Lys-201-CO_2.CABP complex) (*8*) were used for a constrained MD simulation. Structural differences between CABP (an analogue of the six-carbon carboxylated intermediate) and RuBP are minimal, making the substitution of the coordinates of RuBP for CABP relatively straightforward. Removal of the CABP carboxyl moiety removes one of the magnesium ligands. The ligation was restored by a water molecule placed with the guidance of the Rubisco crystal structures for complexes with xylulose 1,5-bisphosphate (XuBP) (*19*) and RuBP (*20*).

To reproduce a complete active site and include all of the protein within 22 Å of the magnesium ion, two large and two small subunits were included in the simulation [each large subunit contained 467 residues and each small subunit contained 123 residues, for a total of 1180 residues plus ligands and magnesiums, giving a total of 12 143 atoms (including united atoms)]. An approximately spherical dynamics zone of radius 22 Å was constructed encompassing

one of the active sites, centered at the Mg ion, with atoms assigned so that the dynamics zone boundary did not cross secondary structure elements. Crystallographic water molecules (279) were included, as well as an additional 28 Å cap of Monte Carlo water molecules (238). The geometry of the magnesium coordination sphere and the binding orientation of the two phosphate groups of RuBP were maintained by half-harmonic potentials. The total number of atoms in the simulation was 13 694, of which 3 291 were in the dynamics zone.

An initial minimization of 50 steps using steepest descent was conducted, followed by a further 500 steps using conjugate gradients. The temperature of the solvent and solute was set initially at 10 K and allowed to warm to 300 K under the influence of the heat bath. The temperature was maintained using the Berendsen coupling algorithm (*21*), with the time constant for the heat bath coupling equal to 0.2 ps. After warming, MD was continued for 1 ns. The root mean square deviations of the backbone and heavy atoms from the crystal structure at this stage were 1.0 and 1.2 Å, respectively. Six sample sets of coordinates were then generated at 5 ps intervals. The two sets with the smallest O2−C2−C3−O3 dihedral angles were then used to produce starting coordinates for a 29-atom active-site fragment. Calculations were performed with both sets at the RHF level to check dependence on the initial coordinates: the relative energies agreed to within 0.1 kcal/mol.

Generation of the Active-Site Fragment. The 29-atom fragment (see Figure 3) was constructed by replacing the Asp-203 and Glu-204 carboxylate groups by formate groups and the carbamylated Lys-201 residue by CH_3NHCOO^-. The substrate was replaced by $C(2)HOC(3)H_2OH$; that is, only the C2 and C3 carbon atoms were included. Several constraints were applied to the fragment: (i) The O3 proton was constrained to the same plane as the C2, C3, and O3 atoms to mimic the hydrogen bond between the substrate and His-294. (ii) The Mg−O3−C3−C2 dihedral angle was constrained to 5° (its value after the initial MD minimization) to balance the torque imposed by the first constraint. (iii) The Mg−carbamate bond was constrained to be perpendicular to the Mg−substrate bonds. (iv) As detailed below, the positions of the Mg ion, the formates, and the water molecule were frozen after an initial minimization.

To minimize the number of atoms in the calculation, we modeled the ketone of RuBP as an aldehyde. This might overestimate the stabilization of the enol form of the substrate (*22*). However, we have also omitted the phosphate groups. The presence of a phosphate group stabilizes the enol tautomer due to the possibility of the hydroxyl proton hydrogen bonding with the bridge O atom of the phosphate group. This would compensate at least in part for the use of the aldehyde.

Calculation of the Reaction Path States. Initially the fragment geometry was partially minimized at the RHF/6-31G(d) level. The formate and water bond distances, angles, and dihedrals were fixed at the values produced by the MD simulation. Geometric parameters for only the substrate fragment, the carbamate fragment, and all of the magnesium−ligand distances were optimized, with the substrate fragment in the initial keto form. The resultant magnesium−formate and magnesium−water distances were fixed at these optimized values for the rest of the calculations. The reason for freezing out these variables was to isolate the electronic energy differences by removing possible perturbations arising from random conformational energy changes. The effect of these restraints on the magnesium−ligand distances was checked by relaxing the restraints in calculations at the RHF/6-31G(d) level and found to affect the relative energies by no more than 0.2 kcal/mol.

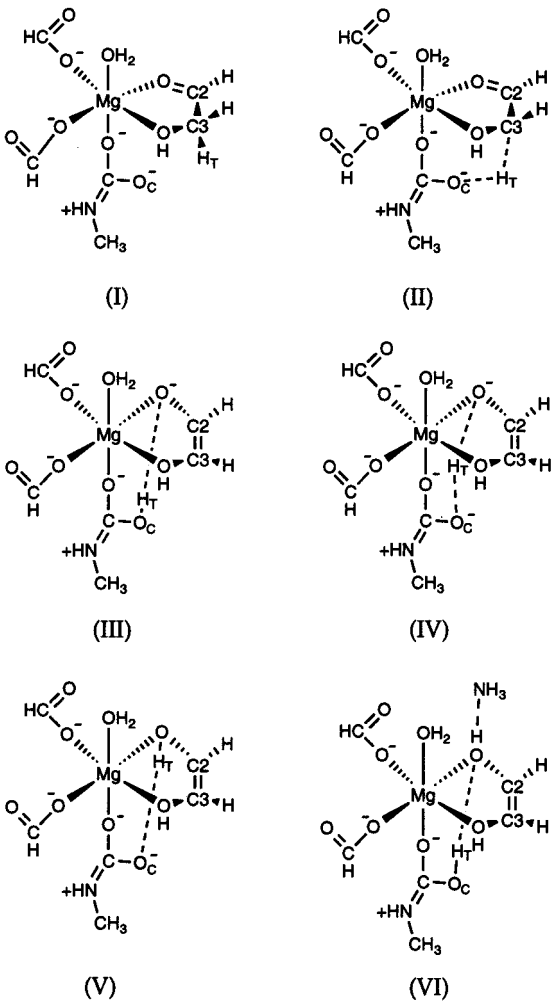

FIGURE 3: States for the 29-atom fragment used to model the enolization of RuBP with geometries optimized at the RHF/6-31+G(d,p) level: (I) substrate in ketone form; (II) transition state structure for the removal of the C3 proton; (III) protonated carbamate H-bonded to the O2 atom [note that no energy minimum was found for the state with protonated carbamate associated with the C3 atom, i.e., the closest structural analogue to state II)]; (IV) transition state structure for the reprotonation of the substrate on O2; (V) substrate in enol form; (VI) enol form (i.e., analogous to state V) for fragment in the presence of an ammonium ion representing Lys-175, with protonated carbamate and ammonium proton transferred to O2. Atoms representing the C2 and C3 atoms of RuBP are labeled.

The 29-atom fragment was optimized in the following states (see Figure 3): (I) the ketone form of the substrate; (II) the transition state associated with removal of the C3 proton; (III) the protonated carbamate form with the proton H-bonded to O2 of the substrate; (IV) the transition state associated with protonation of the enolate form of the substrate; and (V) the enol form of the substrate. Optimization was successful for all of these states. It was not successful for the potential state where protonated carbamate was coordinated to the C3 atom, that is, the potential

Table 1: Relative Energies (kcal/mol) for the Five Reaction Path States of the 29-Atom Fragment (Figure 3) at Different Levels of Calculation

state	RHF/6-31G(d)	RHF/6-31+G(d)	RHF/6-31+G(d,p)	B3LYP/6-31+G(d,p)	MP2/6-31+G(d,p)// RHF/6-31+G(d,p)
I	0.0[a]	0.0[b]	0.0[c]	0.0[d]	0.0[e]
II	36.7	36.9	34.0	18.4	21.5
III	9.9	9.4	5.9		0.1
IV	13.6	13.3	8.9	−1.6[f]	0.1
V	9.7	8.7	5.5		1.8

[a] Zero energy in hartrees is −1162.259160. [b] Zero energy in hartrees is −1162.300871. [c] Zero energy in hartrees is −1162.336163. [d] Zero energy in hartrees is −1168.065058. [e] Zero energy in hartrees is −1165.022582. [f] The optimization of states III and V at the B3LYP/6-31+G(d,p) level results in the same state that resembles state IV.

additional intermediate between intermediates I and III. In this case, either the optimization did not converge or the geometry moved directly to state III, suggesting that the energy barrier between this intermediate and state III is insignificant.

Modeling of Lys-175. To investigate the possible effect of Lys-175 on the enolization reaction and on the whole Rubisco reaction cycle, model calculations were undertaken in which either an ammonium ion or a neutral ammonia molecule was added to the 29-atom fragment in the position of the ϵ-amino group of Lys-175. In the most accurate X-ray structure, the 1.6 Å Rubisco.CABP structure (*8*), the C2 carbon has sp^3 geometry (because of the attached carboxyl group) rather than sp^2 as in the keto form of the substrate. This necessarily changes the orientation of the O2 atom with respect to the ϵ-amino group of Lys-175. A recent lower resolution structure (2.1 Å) of a carbamylated Rubisco.Ca^{2+}.RuBP complex (*20*) might provide better guidance on the positioning of Lys-175 with respect to the substrate. However, to obtain this structure, RuBP was soaked into crystals formed in the presence of the product, PGA, displacing the product. In this structure, loop 6 is still in its retracted position, leaving the active site open to solvent. It has been conjectured that the active site should close when the substrate binds, especially before it is enolized, to prevent water from misprotonating the enol form of RuBP. Perhaps, in this Rubisco.Ca^{2+}.RuBP complex, the active site is held open by crystal forces or by the presence of the nonfunctional metal. If so, this structure may not give an accurate picture of the active site during the enolization process and may not be a reliable guide to the positioning of the amino group. Consequently, in the absence of specific guidance, we positioned the nitrogen atom of the ammonium ion/ammonia molecule in a position 3.2 Å from the O2 atom in the same plane as the O2, C2, and C3 atoms, with an approximately linear H bond, and such that the C2−O2−H(N) angle was an ideal 109°. Although long compared with usual values for O−N heavy-atom distances in H bonds, the 3.2 Å value is a reasonable compromise between the values obtained from the MD simulation and from the carbamylated Rubisco.Ca^{2+}.RuBP structure. The initial coordinates consisted of the optimized 29-atom fragment geometries plus the ammonium ion or ammonia molecule so placed. In the calculations, the positions of only the four or three protons of the ammonium ion or ammonia molecule, respectively, plus the C3 proton being transferred were optimized. Calculations were performed for all five states on the reaction pathway with the ammonium ion but only for states I and II with the ammonia molecule, which was sufficient to check the effect of the charge of the ammonium ion on the activation energy. In addition to these five states, a sixth state (VI; see Figure 3) was optimized in which the ammonium ion proton H-bonded to O2 was moved to the O2 atom and H-bonded to the N atom.

Functional Role of the Carbamate Nitrogen. The necessity for the carbamate structure, in particular the N atom, was investigated by comparison of the relative potential of methylcarbamate to abstract the C3 proton with other small-molecule bases: the simpler parent carbamate (NH_2COO^-), carboxylate groups (propionate, acetate), and bicarbonate. The basicity of the carbamates and the other bases was investigated with simpler magnesium-coordinated structures containing three water molecules and two hydroxyl ions (in positions occupied by the formates in the 29-atom fragment) as the other ligands. These were constructed with idealized octahedral symmetry and magnesium−water and magnesium−hydroxyl bond distances set at 2.1 Å. In the geometry optimizations, only the internal coordinates of the basic fragments were optimized (the orientation of the basic fragment to the hydrated magnesium was fixed), with the coordinates of the magnesium and hydroxyl ions and water molecules frozen. The relative difference in the protonation energies of the fragments was then calculated at the MP2/6-31G(d) level.

In addition, new fragments analogous to the 29-atom fragment were formed by replacing methylcarbamate by the above basic molecules. The geometries of these fragments were reoptimized in states I, II, and III. An ammonium ion was then added as before to form states I, II, III, and VI. The positions of the four ammonium protons and the proton that originated on the C3 atom were optimized as in the previous section. All of these calculations were performed with the smaller basis set 6-31G(d), and then single-point energies of the optimized structures were calculated using MP2 level theory.

RESULTS

Energies on the Reaction Pathway. The relative energies, at different levels of theory, for the 29-atom fragment in the five states along the reaction pathway (Figure 3) are presented in Table 1. These results are without the ammonium ion; corresponding results for the fragment with the ammonium ion are given in Table 2. Relative energies at the RHF level in Table 1 display reasonable convergence with respect to basis set. The addition of diffuse functions causes only small changes (columns 1 and 2). The addition of a p orbital to the hydrogen atoms (column 3) had a larger

Table 2: Relative Energies (kcal/mol) for the Reaction Path States of the 29-Atom Fragment (Figure 3) plus an Ammonium Ion to Model Lys-175[a]

state	RHF/6-31+G(d,p)	B3LYP/6-31+G(d,p)	MP2/6-31+G(d,p)// RHF/6-31+G(d,p)
I	0.0[b]	0.0[c]	0.0[d]
II	30.8	15.0	17.4
III	−5.0	−13.5	−13.0
V	2.7	−5.4	−3.3
VI[e]	−21.7	−24.6	−22.6

[a] See methods for details of geometry parameters optimized. [b] Zero energy in hartrees is −1218.986598. [c] Zero energy in hartrees is −1225.072098. [d] Zero energy in hartrees is −1221.862142. [e] In state VI the carbamate is protonated and the H-bonded proton of the ammonium ion is transferred to O2 leaving an ammonia molecule.

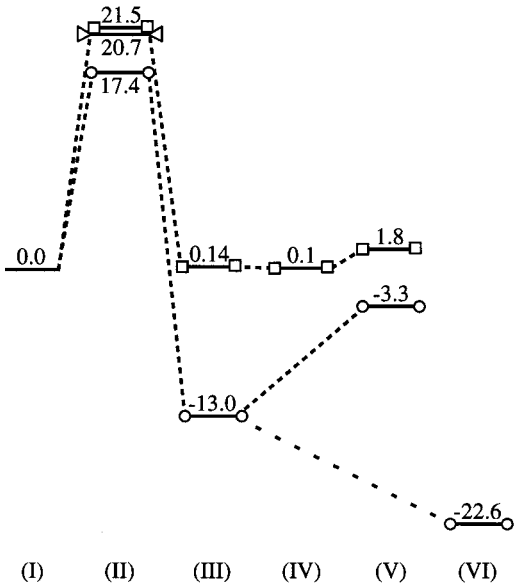

FIGURE 4: Relative energies of the states shown in Figure 3 at the single-point MP2/6-31G(d,p)//RHF/6-31G(d,p) level (see Tables 1 and 2): for the 29-atom fragment, (□); for the 29-atom fragment plus an ammonium ion, (○) or an ammonia molecule, (△) (state II only) modeling Lys-175. State VI has protonated carbamate, protonated O2 atom, and deprotonated ammonium ion.

effect on the relative energies, lowering the activation energy for removal of the proton from 37 to 34 kcal/mol.

Qualitatively, the results of the two methods used to include the effect of electron correlation (MP2 and DFT) agree. They indicate that inclusion of electron correlation is important, with all states being stabilized relative to state I, especially the transition states. The activation energy for the abstraction of the C3 proton is lowered by ∼15 kcal/mol. The DFT calculations show slightly larger electron correlation effects than the MP2 calculations, especially for the transition states. This is not due to the fact that the geometries were optimized, as DFT single-point calculations at the RHF geometries for the transition states (results not shown) also show a larger reduction in activation energy than the MP2 calculations.

Relative energy results for the highest level [MP2/6-31G(d,p)//RHF/6-31G(d,p)] computations are shown graphically in Figure 4. Lines with squares show the energies without the ammonium ion, and lines with circles are the energies with the ammonium ion. The relative energy of states I and II with a neutral ammonia molecule is also shown (triangles). The presence of a neutral ammonia molecule H-bonded to the O2 atom reduces the activation energy of enolization by only a modest 0.8 kcal/mol from 21.5 to 20.7 kcal/mol. However, when a positively charged ammonium ion is H-bonded to the O2 atom, the activation energy is significantly reduced by 4.1 kcal/mol to 17.4 kcal/mol.

Table 3: Comparison of Key Interatomic Distances (in Å) in the Transition State (II) for Abstraction of the C3 Proton (H_T) of Substrate by the Free Oxygen Atom of the Carbamate Group (O_C)[a]

	C3−H_T[b]	O_C−H_T[b]	O_C−C3[b]
without NH_4^+/RHF	1.42	1.25	2.63
without NH_4^+/DFT	1.38	1.32	2.66
with NH_4^+/RHF	1.36	1.33	2.63[c]
with NH_4^+/DFT	1.24	1.48	2.63[c]

[a] Results are given for the 29-atom fragment with and without electron correlation and with and without the ammonium ion (Lys-175) (see Tables 1 and 2). The RHF and DFT calculations were performed using the 6-31+G(d,p) basis set. [b] For definition of H_T and O_C see Figure 3. [c] Heavy atom positions were not optimized with the ammonium ion present.

As is clear from Figure 4, the energies of the enol (state V) and keto (state I) forms for the 29-atom fragment are approximately equal ($\Delta E = 1.8$ kcal/mol). The introduction of the ammonium ion stabilizes the enol form by >20 kcal/mol (state VI) compared with the keto form (state I). In vacuo calculations of the enol and keto forms of the substrate fragment at the MP2/6-31+G(d,p)//RHF/6-31+G(d,p) level indicate that the enol form is ∼10 kcal/mol less stable than the keto form (not shown). This value is comparable with the solution free energy difference for acetaldehyde ($\Delta G = 6.5$ kcal/mol) and acetone ($\Delta G = 9.5$ kcal/mol) (*22*). Consequently, in addition to facilitating the interconversion of the keto form to the enol form, in our active-site model the enol form is stabilized by ∼30 kcal/mol when Lys-175 is protonated or ∼10 kcal/mol when the amino group is not included.

One concern with the results is the large stabilization of the enol form. As the total free energy change of the overall reaction catalyzed by Rubisco is estimated to be −8 or −12 kcal/mol (*23*), an intermediate of energy −22 kcal/mol would be trapped thermodynamically. However, our calculations would overestimate the stability of state VI. These calculations were performed in vacuo. States with high charge separation will be higher in energy than they would be in the actual protein environment. Nevertheless, we expect the qualitative trends of the results to be reliable.

One can see in Figure 4 that, for the 29-atom fragment (without addition of ammonium ion, squares), the states III, IV, and V all have the same energy to within the accuracy of the MP2 calculations. Also, we observe for these states that the carbamate oxygen and O2 atoms are only 2.6 Å away from each other. This structure fits the definition of a strong-short low-barrier hydrogen bond (*24*). However, this structure disappears after the introduction of the ammonium ion, which, in addition to stabilizing the enol form relative to the ketone form, stabilizes the enol form (VI) relative to the enolate (III).

Transition-State Geometry. Key interatomic distances in the transition state for proton abstraction (state II) are presented in Table 3. For the 29-atom fragment (without NH_4^+ ion), the RHF geometry is quite product-like, as shown by the short O−H bond length compared with the C−H bond

Table 4: Differences in Protonation Energies for the Carboxyl Groups of Methylcarbamate, Carbamate, Propionate, Acetate, and Bicarbonate When Coordinated to a Magnesium Ion with Three Water Molecules and Two Hydroxyl Ions as the Other Ligands (See Text)[a]

basic species	ΔE (kcal/mol)	basic species	ΔE (kcal/mol)
$CH_3NHCOO(H)$	0.0[b]	$CH_3CH_2COO(H)$	4.5
$NH_2COO(H)$	1.5	HOCOO(H)	10.6
$CH_3COO(H)$	3.2		

[a] The geometry of the basic ligand only has been optimized at the MP2/6-31G(d) level (see text). [b] Protonation energies are relative to −337.9 kcal/mol.

Table 5: Differences in the Energies of States II, III, and VI Relative to That of State I in the Fragment with an Ammonium Ion, When Methylcarbamate Is Substituted by the Basic Fragments Carbamate, Propionate, Acetate, and Bicarbonate[a]

base	(II) activation energy (kcal/mol)	(III) (kcal/mol)	(VI) (kcal/mol)
CH_3NHCOO^-	0.0[b]	0.0[c]	0.0[d]
NH_2COO^-	1.1	0.3	0.7
CH_3COO^-	1.0	1.5	1.7
$CH_3CH_2COO^-$	1.1	1.8	2.0
$HOCOO^-$	2.5	4.6	8.0

[a] The energies were calculated at the MP2/6-31G(d)//RHF/6-31G(d) level of theory. [b] Energies for state II are relative to 18.9 kcal/mol. [c] Energies for state III are relative to −11.5 kcal/mol. [d] Energies for state VI are relative to −18.6 kcal/mol.

length. When the ammonium ion is added, the transition-state geometry becomes more like that of the reactant. Furthermore, optimization of the transition state using DFT caused both the 29-atom fragment and the fragment with the ammonium ion to be more reactant-like. Thus, the transition-state geometry is more like that of the reactant when electron correlation is included or in the presence of the ammonium ion, conditions which also produce lower transition-state energies and greater stabilization of the product state (III) relative to the reactant state (I).

Functional Role of Carbamate Nitrogen. Protonation energies relative to that of methylcarbamate are presented in Table 4 for the bases (methylcarbamate, carbamate, propionate, acetate, and bicarbonate) coordinated to a hydrated magnesium ion. The differences in the energies of states II, III, and VI relative to state I (in the fragment with ammonium ion) when methylcarbamate is substituted by the same bases are given in Table 5. Both sets of results show the magnitude of the additional stabilization for the various states provided by the methylcarbamate nitrogen atom.

The values in Table 4 show clearly that methylcarbamate and carbamate when simply coordinated to a hydrated magnesium ion are significantly more basic than the simple carboxylates. The results in Table 5 indicate that although this stabilization difference is less for the reaction pathway states with a realistic representation of the active-site magnesium coordination, methylcarbamate is still the most basic. Compared with the corresponding states with the carboxylate bases, states III (i.e., the carbamate-protonated intermediate) and VI (i.e., the carbamate-protonated enol product) are at least 1.5−1.7 kcal/mol more stable when the base is methylcarbamate. For the transition state (II), the difference in the relative energies between the methylcarbamate and carboxylate−base complexes is least; that is, additional stabilization by methylcarbamate of this state is marginal. In summary: magnesium-coordinated methylcarbamate is slightly more basic than carbamate, significantly more basic than propionate and acetate, and much more basic than bicarbonate.

DISCUSSION

Mg-Coordinated Lysyl Carbamate Is Capable of Enolizing RuBP. The primary aim of this work was to assess predictions (*4*, *7*, *8*) that the Mg-coordinated carbamate formed by the carbamylation of Lys-201 during the activation of Rubisco is capable of acting as the base that abstracts the C3 proton. To do this, we calculated the energies of states along a proposed reaction pathway, in which the non-Mg-coordinated carbamate O atom abstracts the C3 proton. The quantum mechanical motion of atoms has been shown to be important in describing proton-transfer reactions (*25*). Zero-point energies tend to lower the activation energy of a proton-transfer reaction (*26*), and the process of tunneling (a purely quantum mechanical process) allows a reaction to occur when classically there is not enough energy. Therefore, as we have omitted these effects from our calculations, the activation energy of 17.4 kcal/mol may be deemed conservatively high. Our calculated activation energies for this proton abstraction support the predictions. The carbamylated lysine residue could indeed be capable of functioning as the general base that facilitates the enolization of RuBP.

Another theoretical study of the enolization of RuBP concluded that direct transfer of the C3 proton to O2 was feasible (*27*). However, this study took no account of the metal or other active-site features. Such a direct transfer mechanism has a high activation energy and would occur just as readily with the C3 epimer, XuBP. Therefore, this mechanism fails to explain the very strong preference Rubisco has for RuBP as substrate compared with XuBP, which reacts only very slowly and eventually causes decarbamylation (*19*, *28*).

At all levels of theory, the rate-limiting step of the enolization of RuBP is the initial abstraction of the proton from the C3 atom, that is, the transition from state I to state III. The activation energy for this step at the simplest level of theory, RHF/6-31G(d), is 36.7 kcal/mol, compared with 3.7 kcal/mol for the abstraction of the proton from the carbamate in the protonation of O2, that is, transition from state III to state V (Table 1). Using DFT, the activation energy for the abstraction of the C3 proton is only 18.4 kcal/mol, but there is no activation energy for the removal of the proton from the carbamate. Therefore, we can expect that active-site groups which stabilize the transition state associated with the proton abstraction (state II) will have the greatest effect on the enolization rate.

Mg-Coordinated Carbamate Is More Basic than Analogous Carboxylates. Such a general-base role is unprecedented for a protein carbamate. Why is the carbamate used in this way? As no activity can occur until the carbamate is formed, it has been suggested that this mechanism could be a device for regulating the activity of Rubisco according to the availability of CO_2 (*29*). It is certainly possible that Rubisco's activity is regulated in this way in some

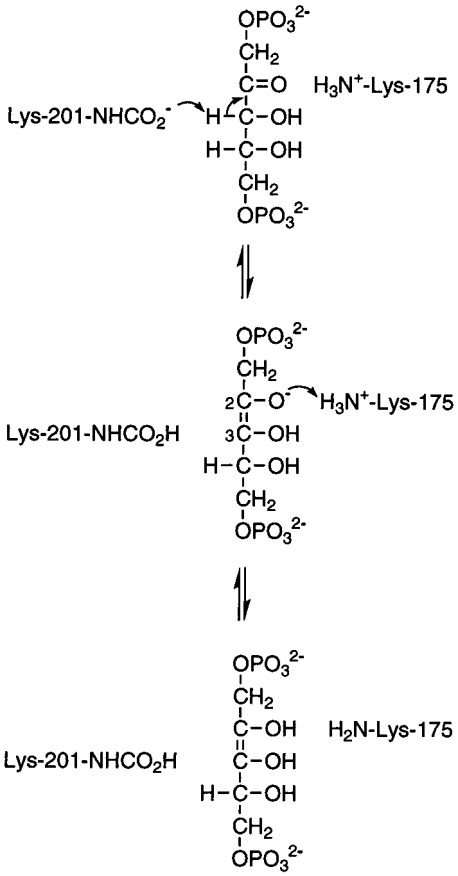

FIGURE 5: Proposed mechanism for the enolization of RuBP. The carbamate group of Lys-201 is the base (B in Figure 1) that deprotonates the C3 atom, while the amino group of Lys-175 initially stabilizes the resultant enolate and then acts as the acid that protonates the O2 atom (A in Figure 1).

organisms. When Rubisco's activity is measured in vitro after pre-equilibration with the same CO_2 concentration used during the activity assay, it shows a clear sigmoidal response to CO_2 concentration that reflects the dual involvement of CO_2 as both cofactor and substrate (*30*). However, in higher plants, Rubisco regulation is quite complex and the influence of CO_2 concentration on activity is masked by another mechanism that involves the release of inhibitors, or of RuBP from the uncarbamylated form of the active site, catalyzed by another chloroplast protein, Rubisco activase (*31*−*33*). Our present calculations provide support for an alternative view that the carbamate is essential to Rubisco's mechanism (see Figure 5) because it performs a role that could not be duplicated by any other group normally found in proteins.

Comparison of the basicity of methylcarbamate with that of other basic fragments, when coordinated to Mg^{2+}, suggests that carbamylated lysine would be ∼4 kcal/mol more basic than glutamate or aspartate (Table 4). This difference was reduced when the basic fragments were incorporated into the larger system. In this case, the difference reduced to 1.5−2 kcal/mol (see calculations for states III and VI in Table 5). Nevertheless, this is still a significant difference in energy that would effectively reduce the enolization rate by more than an order of magnitude and seriously impair the overall rate of catalytic throughput. We note that our argument equates relative protonation energies with relative basicities, that is, enthalpies with free energies. This assumption of similar "solvation" energies is reasonable for the COO moiety among the forms compared.

Role of Lys-175. Several mutants of the *Rodospirillum rubrum* enzyme have been constructed with substitutions at Lys-166 (the residue equivalent to Lys-175 in the spinach enzyme) (*10*). When this residue was mutated to Cys or Gly, the enzyme had 0.15−0.25 and 0.05−0.08% of the enolization activity of the wild-type enzyme, respectively, as measured by enzyme-catalyzed transfer of ^3H radioactivity from [3-^{3}H]RuBP to the medium (*34*). In the enolase structure (*35*), there is a Lys-396 residue that is positioned similarly to Rubisco's Lys-175 residue relative to the enol(ate) that is formed. Mutation of this Lys residue to the sterically similar Met residue reduced the rate of enolization to ∼0.004% of that of wild-type enolase (*36*). The Gly mutant of Rubisco was capable of catalyzing the hydrolysis of the carboxylated intermediate, 3-ketocarboxyarabinitol bisphosphate (3KCABP), but had greatly reduced enolization activity (*9*). The fact that the Gly mutant could be activated, bind CABP, and hydrolyze 3KCABP engenders confidence that these mutants had not undergone large conformational changes. More importantly, this pointed to an important role for Lys-175, specific to the enolization of RuBP.

Prior to the appearance of crystallographic structural information, it had been argued that Lys-175 was the base that abstracted the C3 proton of RuBP (B in Figure 1). This was based in part on the Lys-175 counterpart in *R. rubrum* Rubisco (Lys-166) displaying the unusually low pK_a of 7.9 in its arylation by trinitrobenzenesulfonate (*37*). This pK_a is close to that of an essential base with pK_a = 7.5 observed in the pH dependence of the deuterium isotope effect with [3-^{2}H]RuBP (*38*). However, the remoteness of Lys-175 from C3 precludes its identification as this essential base. Indeed, rather than being the base, Lys-175 may be the essential acid that was detected in the same experiment with a pK_a of 7.9−8.3. Although only the unprotonated form of Lys-175 would be reactive in the arylation reaction, this does not prevent its conjugate acid being the form that is active in the enolization of RuBP. The essential base with a pK_a of 7.5 may be the carbamate itself and/or other residues involved in proton abstractions later in the reaction sequence.

Crystallographic studies have shown that the ϵ-amino atom of Lys-175 is situated near O2 of RuBP, in a position where it could polarize the carbonyl group and perhaps protonate O2 (*11*). In our calculations with the active-site model, a neutral amino group does not significantly lower the activation energy of enolization, whereas a positively charged amino group does. This suggests that, if Lys-175 was initially positively charged, it would significantly stabilize the transition state for proton abstraction. This would explain why mutations at residue 175 cause such large reductions in the enolization rate.

In the active-site model calculations, the lowest energy state is state VI in which a proton from Lys-175 has protonated the O2 atom to complete the enolization process. The next step in the reaction is the addition of CO_2 to the C2 atom. It has been suggested (*4*) that this is facilitated by the removal of the proton on O3. However, if O2 is unprotonated, the deprotonation of O3 would be energetically disfavored and CO_2 would prefer to attack C3 rather than C2. This alternative carboxylation has not been observed with Rubisco. Therefore, we suggest that Lys-175 is the

acidic group (A in Figure 1) that protonates O2 and thus plays an important role in directing CO_2 attack to C2. This postulated role requires that Lys-175 be in the protonated form at the commencement of the reaction (see Figure 5). However, protonation of O2 to form the enediol does not by itself direct CO_2 attack toward C2. Deprotonation of O3 is also required (see later).

Our suggestion that Lys-175 is positively charged at the start of the reaction is consistent with the available mutagenesis data. In the two *R. rubrum* Rubisco mutants Lys was replaced by a smaller residue, Gly or Cys (*34*). Therefore, one might expect the resultant void to be occupied by water. The activity of the Gly mutant is lower than that of the Cys mutant. This may be a result of the greater main-chain flexibility allowed by Gly and consequent local conformational changes. The water replacing the amino side chain would still be able to hydrogen bond with the O2 atom, and thus these two mutants would correspond to our fragment with NH_3. The difference in the effective activation free energy, inferred from the reductions in the rates, is ~3.5−4.5 kcal/mol for these two mutants. We can compare this difference with the activation energy differences in our calculations. The experimental change in activation free energy does correspond approximately to the difference in activation energy between NH_4^+ and NH_3, which is 3.3 kcal/mol in our calculations (Figure 4).

We can apply the same analysis to the enolase mutant (*36*). When Lys is mutated to Met, the change in the effective activation free energy suggested by the rate reduction is ~6 kcal/mol (*36*). The replacement of the positively charged amino group by an apolar Met side chain is chemically analogous to the removal of the NH_4^+ completely. The difference between our calculated activation energy with NH_4^+ and the simple 29-atom fragment without NH_4^+ or NH_3 is 4.1 kcal/mol (Figure 4).

The substitutions for Lys would be expected to cause local conformational perturbations in addition to the elimination of the residue's acidity, and these would be expected to increase the free energy changes beyond those estimated by our calculations. Thus, we consider that there is good agreement between the data for the Rubisco and enolase mutants and our calculations regarding the likely effect of protonated Lys on the enolization rate. The performance of the mutants can be divided into two categories—if the protonated amino group is replaced by something polar, such as water or NH_3, enolization is reduced 400−2000-fold; if it is replaced by something apolar, a 25000-fold reduction occurs.

A recent review (*4*) presented a mechanism in which Lys-175 is neutral at the start of the reaction. Our calculations enable an assessment of some of the steps of this mechanism. In particular, the mechanism involves a step in which a proton moves from O2 of the enediol to Lys-175. In that mechanism, the carbamate is deprotonated at this stage of the reaction and, thus, unable to hydrogen bond with the negatively charged O2 as it does in our model calculations. This step, except for the protonation state of the carbamate, is equivalent to moving from state VI to state III. Our calculations indicate that such a step would be very unfavorable energetically, and the deprotonated carbamate would make it even more so. Therefore, we consider that this aspect of the mechanism proposed by Cleland et al. (*4*) is improbable.

Consequences of the Proposed Enolization Mechanism for Subsequent Catalytic Steps. Our suggested mechanism for enolization leaves Lys-175 unprotonated, the substrate fully enolized, and the carbamate protonated. It is important to consider the consequences of these finishing conditions on subsequent catalytic steps. One potential problem is presented by the protonated state of the carbamate—obviously it cannot be used again for proton abstraction later in the reaction sequence. Two further protons need to be abstracted to enable the reaction to complete. The first must come from O3 to allow CO_2 to attack at C2. His-294 seems ideally positioned to carry out this task (*20*). Second, a water molecule must be deprotonated so that the resultant hydroxide ion can attack C3 to hydrate the 3-ketoacid produced by carboxylation at C2. Whether this attack occurs in concert with CO_2 attack or subsequently (*39*) would be an interesting topic for a future computational study. In any event, another histidyl residue, His-327, is well positioned to deprotonate the water molecule (*20*). Because of their proximity, it is unlikely that His-294 and His-327 could be both protonated at the same time. However, both are in contact with other residues that could distribute the charge. C2−C3 cleavage of the *gem*-diol form of the carboxylated intermediate would then be initiated by the negative charge on O3.

The neutral state of Lys-175 after enolization presents another potential difficulty because this residue has been shown by mutagenesis to mediate the protonation of C2 of the three-carbon *aci*-acid intermediate produced from carbons 1 and 2 and the CO_2 molecule (*13*). Although Lys-175 obviously participates in this protonation reaction, it may not be the ultimate source of the proton. For example, because the C2 atom of the *aci*-acid is now very basic, movement of the proton attached to O2 via Lys-175 to C2 would be favorable thermodynamically. The positions of the heavy atoms seem well suited for such a shuttle. A computational study of this step in vacuo, without taking active-site residues into account, indicated that O2 was likely to be involved in trafficking this proton (*40*). Although the carbamate proton that was derived from C3 is the ultimate acid in this shuttle, that particular proton would travel only as far as O2. There it would be exchangeable, in keeping with observations that isotopic label in the C3 proton of RuBP does not appear in products (*41*). Thus, neither the protonated state of the carbamate nor the unprotonated state of Lys-175 that results from the proposed enolization mechanism appears to present insuperable difficulties to subsequent catalytic steps.

Involvement of His-294 in Enolization. If, as we and others (*20*) suggest, the role of the side chain of His-294 is to accept the proton from O3 of the enediol in the step immediately following enolization, then it is not obvious that this residue should have a direct role in enolization itself. Nevertheless, mutation of His-294 severely impairs both enolization and overall catalysis (*42*, *43*). It has recently been proposed that His-294 might assist enolization by hydrogen bonding to the protonated form of carbamylated Lys-201, effectively increasing the basicity of the carbamate (*43*). This possibility is not excluded by our calculations and might be an interesting topic for future study. Thus, the functions of His-294 and Lys-175 would combine to produce the particular enediolate tautomer required to direct CO_2 attack to C2 rather than to C3.

Reliability of the Active-Site Model. For the purposes of the current study of the first reaction step of Rubisco, we have carried out high-level quantum chemical calculations on a limited fragment centered around the active-site Mg atom. However, the overall mechanism is very complex, and the active site has many ionizable groups and also contains water molecules. Ideally we would like to be able to model the reaction steps using a full description of the enzyme environment, including solvent. Methods to undertake such studies on enzyme reactions using either hybrid quantum mechanics/molecular mechanics treatments (*44*) or full quantum mechanical models using linear scaling (*45*) have been reported and applied recently to simple systems, including by us (*46*, *47*). However, such applications require a detailed knowledge of the ionization states of active-site groups, as well as the locations of the bound water molecules, which need to be obtained from experiment and complemented by preliminary simulations. For Rubisco, this level of definition is not yet available, but some of the necessary issues have been addressed in the current study.

Conclusion. Our calculations suggest a mechanism (Figure 5) by which Rubisco catalyzes the enolization of RuBP that is consistent with all experimental evidence available. The carbamate formed during the activation of Rubisco acts as the base in Figure 1 and deprotonates the C3 atom. The developing charge on the carbonyl O atom is first stabilized by the positively charged Lys-175 residue and then protonated by it. Thus, Lys-175 plays the role of the acid in Figure 1. In this respect, our proposed mechanism for RuBP enolization differs from that described by Cleland et al. (*4*), who proposed that the proton is directly transferred from C3 to O2 by the lysyl carbamate alone.

REFERENCES

1. Andrews, T. J., and Lorimer, G. H. (1987) in *The Biochemistry of Plants: A Comprehensive Treatise, Vol. 10, Photosynthesis* (Hatch, M. D., and Boardman, N. K., Eds.) pp 131−218, Academic Press, New York.
2. Hartman, F. C., and Harpel, M. R. (1994) *Annu. Rev. Biochem. 63*, 197−234.
3. Gutteridge, S., and Gatenby, A. A. (1995) *Plant Cell 7*, 809−819.
4. Cleland, W. W., Andrews, T. J., Gutteridge, S., Hartman, F. C., and Lorimer, G. H. (1998) *Chem. Rev. 98*, 549−561.
5. Knowles, J. R. (1991) *Nature 350*, 121−124.
6. Babbitt, P. C., Hasson, M. S., Wedekind, J. E., Palmer, D. R. J., Barrett, W. C., Reed, G. H., Rayment, I., Ringe, D., Kenyon, G. L., and Gerlt, J. A. (1996) *Biochemistry 35*, 16489−16501.
7. Newman, J., and Gutteridge, S. (1993) *J. Biol. Chem. 268*, 25876−25886.
8. Andersson, I. (1996) *J. Mol. Biol. 259*, 160−174.
9. Lorimer, G. H., and Hartman, F. C. (1988) *J. Biol. Chem. 263*, 6468−6471.
10. Hartman, F. C., Soper, T. S., Niyogi, S. K., Mural, R. J., Foote, R. S., Mitra, S., Lee, E. H., Machanoff, R., and Larimer, F. W. (1987) *J. Biol. Chem. 262*, 3496−3501.
11. Lundqvist, T., and Schneider, G. (1991) *J. Biol. Chem. 266*, 12604−12611.
12. Knight, S., Andersson, I., and Branden, C.-I. (1990) *J. Mol. Biol. 215*, 113−160.
13. Harpel, M. R., and Hartman, F. C. (1996) *Biochemistry 35*, 13865−13870.
14. Pearlman, D. A., Case, D. A., Caldwell, J. W., Ross, W. S., Cheatham, T. E., III, Ferguson, D. M., Seibel, G. L., Singh, C. U., Weiner, P. K., and Kollman, P. A. (1995) AMBER 4.1, University of California, San Francisco.
15. Jorgensen, W. L., and Tirado-Rives, J. (1988) *J. Am. Chem. Soc. 110*, 1657−1666.
16. Frisch, M. J., Trucks, G. W., Schlegel, H. B., Gill, P. M. W., Johnson, B. G., Robb, M. A., Cheeseman, J. R., Keith, T. A., Petersson, G. A., Montgomery, J. A., Raghavachari, K., Al-Laham, M. A., Zakrzewski, V. G., Ortiz, J. V., Foresman, J. B., Peng, C. Y., Ayala, P. A., Wong, M. W., Andres, J. L., Replogle, E. S., Gomperts, R., Martin, R. L., Fox, D. J., Binkley, J. S., Defrees, D. J., Baker, J., Stewart, J. P., Head-Gordon, M., Gonzalez, C., and Pople, J. A. (1995) Gaussian 94 (revision E.2), Gaussian, Inc., Pittsburgh, PA.
17. Cerjan, C. J., and Miller, W. H. (1981) *J. Chem. Phys. 75*, 2800−2806.
18. Becke, A. D. (1993) *J. Chem. Phys. 98*, 5648−5652.
19. Newman, J., and Gutteridge, S. (1994) *Structure 2*, 495−502.
20. Taylor, T. C., and Andersson, I. (1997) *J. Mol. Biol. 265*, 432−444.
21. Berendsen, H. J. C., Postma, J. P. M., van Gunsteren, W. F., DiNola, A., and Haak, J. R. (1984) *J. Chem. Phys. 81*, 3684−3690.
22. Streitwieser, A., Jr., and Heathcock, C. H. (1985) *Introduction to Organic Chemistry*, 3rd ed., p 367, Macmillan Publishing, New York.
23. Heldt, H.-W. (1997) *Plant Biochemistry and Molecular Biology*, p 151, Oxford University Press, Oxford, U.K. Stryer, L. (1981) *Biochemistry*, 2nd ed., p 445, W. H. Freeman, New York.
24. Gerlt, J. A., Kreevoy, M. M., Cleland, W. W., and Frey, P. A. (1997) *Chem. Biol. 4*, 259−267.
25. Hwang, J.-K., and Warshel, A. (1996) *J. Am. Chem. Soc. 118*, 11745−11751.
26. Hehre, W. J., Radom, L., Schleyer, P. v. R., and Pople, J. A. (1986) *Ab Initio Molecular Orbital Theory*, Wiley, New York.
27. Tapia, O., Andres, J., and Safont, V. S. (1994) *J. Phys. Chem. 98*, 4821−4830.
28. Yokota, A. (1991) *Plant Cell Physiol. 32*, 755−762.
29. Schloss, J. V. (1990) in *Enzymatic and Model Carboxylation and Reduction Reactions for Carbon Dioxide Utilization* (Aresta, M., and Schloss, J. V., Eds.) pp 321−345, Kluwer Academic Publishers, Dordrecht, The Netherlands.
30. Andrews, T. J., and Hatch, M. D. (1971) *Phytochemistry 10*, 9−15.
31. Portis, A. R., Jr. (1992) *Annu. Rev. Plant Physiol. Plant Mol. Biol. 43*, 415−437.
32. Mate, C. J., von Caemmerer, S., Evans, J. R., Hudson, G. S., and Andrews, T. J. (1996) *Planta 198*, 604−613.
33. Salvucci, M. E., and Ogren, W. L. (1996) *Photosynth. Res. 47*, 1−11.
34. Hartman, F. C., and Lee, E. H. (1989) *J. Biol. Chem. 264*, 11784−11789.
35. Lebioda, L., and Stec, B. (1991) *Biochemistry 30*, 2817−2822.
36. Reed, G. H., Poyner, R. R., Larsen, T. M., Wedekind, J. E., and Rayment, I. (1996) *Curr. Opin. Struct. Biol. 6*, 736−743.
37. Hartman, F. C., Milanez, S., and Lee, E. H. (1985) *J. Biol. Chem. 260*, 13968−13975.
38. Van Dyk, D. E., and Schloss, J. V. (1986) *Biochemistry 25*, 5145−5156.
39. Cleland, W. W. (1990) *Biochemistry 29*, 3194−3197.
40. Safont, V. S., Oliva, M., Andres, J., and Tapia, O. (1997) *Chem. Phys. Lett. 278*, 291−296.
41. Fiedler, F., Müllhofer, G., Trebst, A., and Rose, I. A. (1967) *Eur. J. Biochem. 1*, 395−399.
42. Lorimer, G. H., Gutteridge, S., and Madden, M. W. (1987) *Plant Molecular Biology* (von Wettstein, D., and Chua, N. H., Eds.) pp 21−31, Plenum Press, New York.
43. Harpel, M. R., Larimer, F. W., and Hartman, F. C. (1998) *Protein Sci. 7*, 730−738.
44. Eurenius, K. P., Chatfield, D. C., Brooks, B. R., and Hodoscek, M. (1996) *Int. J. Quantum Chem. 60*, 1189−1200.
45. Stewart, J. J. P. (1996) *Int. J. Quantum Chem. 58*, 133−146.
46. Ranganathan, S., and Gready, J. E. (1997) *J. Phys. Chem. B 101*, 5614−5618.
47. Cummins, P. L., and Gready, J. E. (1998). *J. Comput. Chem. 19*, 977−988.

BI981598E